Frontiers of Information Technology & Electronic Engineering
www.zju.edu.cn/jzus; engineering.cae.cn; www.springerlink.com
ISSN 2095-9184 (print); ISSN 2095-9230 (online)
E-mail: jzus@zju.edu.cn

Orbit determination using incremental phase and TDOA of X-ray pulsar*

Rong JIAO, Lu-ping XU†‡, Hua ZHANG, Cong LI

(*School of Aerospace Science and Technology, Xidian University, Xi'an 710126, China*)

†E-mail: lpxu@mail.xidian.edu.cn

Received Oct. 26, 2015; Revision accepted Mar. 22, 2016; Crosschecked May 14, 2016

Abstract: X-ray pulsars offer stable, periodic X-ray pulse sequences that can be used in spacecraft positioning systems. A method using X-ray pulsars to determine the initial orbit of a satellite is presented in this paper. This method suggests only one detector to be equipped on the satellite and assumes that the detector observes three pulsars in turn. To improve the performance, the use of incremental phase in one observation duration is proposed, and the incremental phase is combined with the time difference of arrival (TDOA). Then, a weighted least squares (WLS) algorithm is formulated to calculate the initial orbit. Numerical simulations are performed to assess the proposed orbit determination method.

Key words: Orbit determination algorithm, Single X-ray pulsar detector, Phase increment, Two-body motion equations, Weighted least squares method

http://dx.doi.org/10.1631/FITEE.1500365 **CLC number:** V44; TP872

1 Introduction

The determination of the orbit is one of the important tasks in spacecraft operations and control. The knowledge of the orbit parameters is an essential part for the spacecraft mission such as data analysis, mapping, and communication. Traditionally, ground-based orbit determination is used. Several researchers have shown that the low-Earth-orbit elements can be obtained by using the global positioning system (GPS) (Visser and van den Ijssel, 2000), and deep space missions, where the GPS signal cannot be received, are served by the deep space network (DSN) (Hinedi, 1993). However, the ground-based method is nonautonomous and very expensive because the spacecraft receives the signal from a man-made facility for estimation and control of its trajectory. To achieve more autonomy and reduce the dependence of the orbit determination system on a ground-based operation, the use of celestial-based orbit determination systems has been suggested. These methods allow the spacecraft to self-determine their own orbit elements relying on celestial sources, such as stars (Ma *et al.*, 2005; Xiong *et al.*, 2013), planetoids (Qian *et al.*, 2013), or the Earth's magnetic field (Psiaki, 1995; Deutschmann and Bar-Itzhack, 2001). In general, the traditional celestial orbit determination method employs the geometry information of the sources, e.g., the angle between the star and the Earth's center or the spatial distribution of the magnetic intensity (Psiaki, 1995; Deutschmann and Bar-Itzhack, 2001; Ma *et al.*, 2005; Qian *et al.*, 2013; Farahanifar and Assadian, 2015). The performance of this method is heavily dependent on the distance and angle relating to the Earth's center, and most of these methods are used mainly in low-Earth-orbit missions. In contrast, orbit

‡Corresponding author

* Project supported by the National Natural Science Foundation of China (No. 61401340), the Natural Science Basic Research Plan in Shaanxi Province of China (No. 2016JM6035), the Fundamental Research Funds for the Central Universities, China (No. JB161303), and the Areospace T.T.&C. Innovation Program (No. 201515A)

ORCID: Rong JIAO, http://orcid.org/0000-0002-3409-2826

determination using the timing information from the variable celestial method has been developed recently. Specifically, due to their special characteristics, one of the variable celestial bodies, namely X-ray pulsars, is a potential candidate for use in modern autonomous orbit determination systems. It was first proposed by Chester and Butman (1981), who named it X-ray pulsar navigation (XNAV).

Pulsars are highly magnetized rotating neutron stars, which emit periodic pulses of electromagnetic radiation. These pulses have a unique profile, and are characterized by extremely high stability and regularity. A detector placed in the beam of the pulsar radiation can reconstruct the pulse and measure the time of arrival (TOA), which can be used to determine the position by calculating the flying time of the pulse between the detector and the solar system barycenter (SSB). This principle is similar to GPS, which obtains the distance by measuring the time difference between the satellite and the receiver. Thus, XNAV is called a 'natural global positioning system'. Several researchers have introduced this technology (Ray *et al.*, 2002; Sheikh *et al.*, 2011; Zhang *et al.*, 2014). According to some, one of the major applications of XNAV is to determine the orbit of the spacecraft (Woodfork, 2005; Huang and Liang, 2010; Mao *et al.*, 2010). Woodfork (2005) used the time difference of arrival (TDOA) between the satellites to aid GPS satellite orbit determination. The use of X-ray pulsar to make the initial orbit determination of the high Earth orbit was introduced by Huang and Liang (2010). Orbit determination by a single X-ray pulsar was discussed by Mao *et al.* (2010). These works show that an accuracy of only several hundred meters can be obtained using the state-of-the-art technology. Some improved methods, which employ additional resources such as the Sun or stars, have been proposed (Ray *et al.*, 2002; Liu *et al.*, 2015). These methods require a subsystem to deal with the additional inputs, which increases the complexity and burden of the navigation system. In view of the above, we present a novel method in this paper that addresses the use of one single pulsar to determine the initial orbit. This method assumes that the detector points to three pulsars in turn, and proposes to use the increment of the pulse phase brought in by satellite movement to improve the precision of orbit determination. Then, the weighted least squares (WLS) algorithm is integrated with the TDOA and the increment phase, which can provide more information than the traditional XNAV.

2 Basic principle of pulsar navigation

X-ray pulsar navigation uses the X-ray pulse's TDOA between the spacecraft and the SSB to determine spacecraft's position and velocity (Sheikh, 2005; Wang *et al.*, 2013). To obtain the TDOA, the measured pulse TOA at the satellite should be compared with the predicted pulse TOA at the SSB (Sheikh *et al.*, 2007; Emadzadeh and Speyer, 2011; Zhang and Xu, 2011).

The TOA of a photon recorded by an atomic clock is a proper time. To compare the TOA of the measured pulse and the TOA of the predicted pulse in the same time framework, the proper time must be transformed to a coordinate time such as the barycentric coordinate time (TCB) or barycentric dynamic time (TDB) (Sheikh, 2005; Sheikh *et al.*, 2007; Shang *et al.*, 2013). TCB is adopted in this study.

The barycenter of the solar system's celestial reference system (BCRS) is established (Fig. 1), with the barycenter of the solar system $\boldsymbol{O}_{\mathrm{SSB}}$ as the origin, $\boldsymbol{X}_{\mathrm{SSB}}$ pointing to the vernal point defined by the standard epoch J2000.0, and $\boldsymbol{Z}_{\mathrm{SSB}}$ is perpendicular to the celestial equator and $\boldsymbol{Y}_{\mathrm{SSB}}$ is pointing to the *X*-*Z* plane according to the right-hand rule. $\boldsymbol{O}_{\mathrm{E}}$ and $\boldsymbol{O}_{\mathrm{Sun}}$ are the mass centers of the Earth and Sun, respectively. $\boldsymbol{R}_{\mathrm{SC}}$, $\boldsymbol{D}$, $\boldsymbol{R}_{\mathrm{E}}$, and $\boldsymbol{b}$ are the position vectors of satellite, pulsar, and center mass of the Earth and Sun with respect to SBB, respectively. Variables λ, α, and $\boldsymbol{n}$ are the right ascension, declination, and the radiation direction of pulsar, respectively.

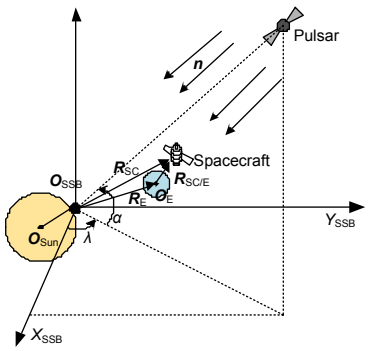

Fig. 1 Geometric relationships among pulsars, Earth, Sun, and the spacecraft

In the BCRS, the space-time coordinates of the spacecraft are assumed as (Backer and Hellings, 1986; Sheikh, 2005)

$$\{ct, x, y, z\} = \{x^0, x^1, x^2, x^3\}, \quad (1)$$

where c is the light speed and the space-time interval is

$$\mathrm{d}s^2 = \sum_{p,q} g_{pq} \mathrm{d}x^p \mathrm{d}x^q, \quad p, q = 1, 2, 3, 4, \quad (2)$$

where g_{pq} is the metric tensor and a function of time and space coordinates, which determines the nature of space.

Because the ratio between the gravitational radius of the Sun and its physical radius is only 10^{-6} (Sheikh, 2005), the solar system can be regarded as a weak gravitational field and its time and space are nearly the flat Minkowski space-time. Thus, the second-order post-Newtonian metric tensor is suitable, and only the lower-order terms of the space-time metric components need to be retained. Then, the space-time interval can be written as

$$\mathrm{d}s^2 = \left(1 - \frac{2U}{c^2}\right) c^2 \mathrm{d}t^2 - \left(1 + \frac{2U}{c^2}\right)(\mathrm{d}x^2 + \mathrm{d}y^2 + \mathrm{d}z^2), \quad (3)$$

where $U = \sum_i \mathrm{Gm}_i / r_i$ represents the sum of the gravitational potentials of all celestial bodies generated at the onboard clock in the solar system, Gm_i is the gravitational constant of the ith celestial body, and r_i is the distance between the ith celestial body and the spacecraft.

The distance between the pulsar and the solar system is as much as thousands of light years, so the pulsar radiation direction can be approximately regarded as a constant vector in the whole solar system. Taking into account that the gravity of the Sun is the main gravity source in the solar system, the simplified TOA transfer equation from the spacecraft to the SSB was given by Ray *et al.* (2002), Sheikh (2005), and Taylor (1992), as

$$\begin{aligned} t_{\mathrm{SSB}} - t_{\mathrm{SC}} &= \frac{\boldsymbol{n} \cdot \boldsymbol{R}_{\mathrm{SC}}}{c} + \frac{1}{2cD_0}\left[(\boldsymbol{n} \cdot \boldsymbol{R}_{\mathrm{SC}})^2 - \|\boldsymbol{R}_{\mathrm{SC}}\|^2 \right. \\ &\left. + 2(\boldsymbol{n} \cdot \boldsymbol{b})(\boldsymbol{n} \cdot \boldsymbol{R}_{\mathrm{SC}}) - 2\boldsymbol{b} \cdot \boldsymbol{R}_{\mathrm{SC}}\right] \\ &+ \frac{2\mu_{\mathrm{s}}}{c^3} \ln \left| \frac{\boldsymbol{n} \cdot \boldsymbol{R}_{\mathrm{SC}} + \boldsymbol{n} \cdot \boldsymbol{b} + \|\boldsymbol{R}_{\mathrm{SC}}\| + \|\boldsymbol{b}\|}{\boldsymbol{n} \cdot \boldsymbol{b} + \|\boldsymbol{b}\|} \right|, \end{aligned} \quad (4)$$

where t_{SSB} and t_{SC} are the TOA of the SSB and the satellite, respetively, μ_{s} the gravity of the Sun, $\boldsymbol{R}_{\mathrm{SC}}$ and $\boldsymbol{b}$ the position vectors of the satellite and the Sun with respect to SSB, respectively, $\boldsymbol{n}$ the angular position vector of the pulsar, and D_0 the distance between the first pulsar and SSB.

The pulse timing model defined at the SSB can be expressed as

$$\phi(t) = \phi(t_0) + f(t - t_0) + \sum_{n=2}^{+\infty} \frac{f^{n-1}(t - t_0)^n}{n!}, \quad (5)$$

where $\phi(t)$ is the phase of the pulsar at time t in SSB, t_0 the reference epoch, and f the pulse frequency. Then, t_{SSB} can be obtained as

$$t_{\mathrm{SSB}} = \arg(\phi_{\mathrm{SSB}}(t)), \quad (6)$$

where $\arg(\cdot)$ indicates extracting time from ϕ_{SSB}, or

$$t_{\mathrm{SSB}} = \phi_{\mathrm{SSB}} P, \quad (7)$$

where P is the period of pulsar and ϕ_{SSB} the phase between the pulsar and the solar system's barycenter at time t. In a similar way, we have

$$t_{\mathrm{SC}} = \phi_{\mathrm{SC}} P, \quad (8)$$

where ϕ_{SC} is the phase between the pulsar and the satellite at time t_{SC}. Substituting Eqs. (7) and (8) into Eq. (4), the time delay from SSB to the satellite, t_{d}, can be rewritten as

$$\begin{aligned} t_{\mathrm{d}} = \psi \cdot P = \tilde{t} + \delta t &= \frac{\boldsymbol{n} \cdot \boldsymbol{R}_{\mathrm{SC}}}{c} \\ &+ \frac{1}{2cD_0}\left[(\boldsymbol{n} \cdot \boldsymbol{R}_{\mathrm{SC}})^2 - \|\boldsymbol{R}_{\mathrm{SC}}\|^2 + 2(\boldsymbol{n} \cdot \boldsymbol{b})(\boldsymbol{n} \cdot \boldsymbol{R}_{\mathrm{SC}}) - 2\boldsymbol{b} \cdot \boldsymbol{R}_{\mathrm{SC}}\right] \\ &+ \frac{2\mu_{\mathrm{s}}}{c^3} \ln \left| \frac{\boldsymbol{n} \cdot \boldsymbol{R}_{\mathrm{SC}} + \boldsymbol{n} \cdot \boldsymbol{b} + \|\boldsymbol{R}_{\mathrm{SC}}\| + \|\boldsymbol{b}\|}{\boldsymbol{n} \cdot \boldsymbol{b} + \|\boldsymbol{b}\|} \right|, \end{aligned} \quad (9)$$

where $\psi = \phi_{\mathrm{SSB}} - \phi_{\mathrm{SC}}$ is the phase between SSB and the satellite, $\tilde{t} = (\boldsymbol{n} \cdot \boldsymbol{r}) / c$ is the time delay caused by the geometric distance, and δt is the time delay caused by

the parallel arrival of X-rays in the solar system and relativistic effect. δt can be written as

$$\delta t = -\frac{1}{2cD_0}\left[(\boldsymbol{n}\cdot\boldsymbol{R}_{\mathrm{SC}})^2-\|\boldsymbol{R}_{\mathrm{SC}}\|^2+2(\boldsymbol{n}\cdot\boldsymbol{b})(\boldsymbol{n}\cdot\boldsymbol{R}_{\mathrm{SC}})-2\boldsymbol{b}\cdot\boldsymbol{R}_{\mathrm{SC}}\right] -\frac{2\mu_{\mathrm{s}}}{c^3}\ln\left|\frac{\boldsymbol{n}\cdot\boldsymbol{R}_{\mathrm{SC}}+\boldsymbol{n}\cdot\boldsymbol{b}+\|\boldsymbol{R}_{\mathrm{SC}}\|+\|\boldsymbol{b}\|}{\boldsymbol{n}\cdot\boldsymbol{b}+\|\boldsymbol{b}\|}\right|. \tag{10}$$

The TOA observation of XNAV is obtained as

$$\boldsymbol{Z}=[t_1\ t_2\ t_3\ \cdots], \tag{11}$$

where t_1, t_2, t_3, … are the time delays from SSB to the satellite at different instants.

3 Incremental phase of the pulsar signal

In XNAV, the basic measurement can be simply defined as the time delay between the satellite and SSB, which is calculated from the TOA of the pulsar signals, as shown in the previous section. Here, phase increment measurement is used to improve the accuracy of the traditional XNAV. The phase increment arises from the movement of the detector fixed on the satellite (Fig. 2).

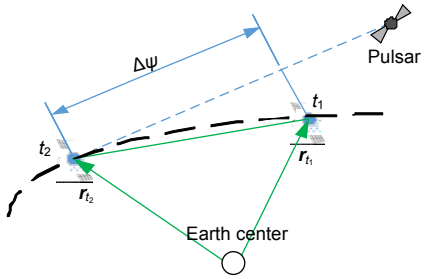

Fig. 2 Geometric model of time increment observation

In Fig. 2, t_1 and t_2 denote two instants of the satellite orbit, and the phase difference between the two instants can be expressed as

$$\Delta\psi=\psi_{t_2}-\psi_{t_1}, \tag{12}$$

where ψ_{t_1} and ψ_{t_2} denote the phase between the pulsar and the satellite at time t_1 and t_2, respectively. $\boldsymbol{r}_{t_1}$ and $\boldsymbol{r}_{t_2}$ are the position vectors of the satellite at t_1 and t_2 with respect to the Earth center, respectively.

According to Eq. (4), $\Delta\psi$ can be derived from the position vectors $\boldsymbol{r}_{t_1}$ and $\boldsymbol{r}_{t_2}$ as

$$\Delta t=\Delta\psi P=\frac{\boldsymbol{n}\cdot(\boldsymbol{r}_{t_2}-\boldsymbol{r}_{t_1})}{c}-\frac{1}{2cD_0}\left[(\boldsymbol{n}\cdot(\boldsymbol{r}_{t_1}+\boldsymbol{r}_{t_2}))(\boldsymbol{n}\cdot\delta\boldsymbol{r}) -(\|\boldsymbol{r}_{t_1}\|+\|\boldsymbol{r}_{t_2}\|)\|\delta\boldsymbol{r}\|+2(\boldsymbol{n}\cdot\boldsymbol{b})(\boldsymbol{n}\cdot\delta\boldsymbol{r})-2\boldsymbol{b}\cdot\delta\boldsymbol{r}\right] -\frac{2\mu_{\mathrm{s}}}{c^3}\ln\left|1+\frac{\boldsymbol{n}\cdot\delta\boldsymbol{r}+\|\delta\boldsymbol{r}\|}{\boldsymbol{n}\cdot\boldsymbol{r}_{t_1}+\boldsymbol{n}\cdot\boldsymbol{b}+\|\boldsymbol{r}_{t_1}\|+\|\boldsymbol{b}\|}\right|, \tag{13}$$

where $\delta\boldsymbol{r}=\boldsymbol{r}_{t_2}-\boldsymbol{r}_{t_1}$.

Generally, the distance between the satellite and SSB (r=$\|\boldsymbol{r}\|$) is on the order of 10^7 km, while that between the center of the Sun and SSB (b=$\|\boldsymbol{b}\|$) is on the order of 10^6 km. However, in the solar system, D_0 is on the order of 10^{14} km. Assuming that the observation time of TOA is 500 s and that the speed of the satellite is 7.9 km/s, the position increment $\|\delta\boldsymbol{r}\|$ between the adjoining instants is in the order of 10^2 km. Therefore, the values of $(\|\boldsymbol{r}_{t_1}\|+\|\boldsymbol{r}_{t_2}\|)\|\delta\boldsymbol{r}\|/D_0$ with the order of magnitude 10^{-6} and $(\boldsymbol{n}\cdot\boldsymbol{b})(\boldsymbol{n}\cdot\delta\boldsymbol{r})/D_0$ with the order of magnitude 10^{-7} are negligible. As the distance between the satellites at two different instants is relatively small, the effects caused by the parallel X-rays and the relativistic effects are roughly the same, and the common error terms in the TOA can be eliminated at the adjacent moments of the satellite. Thus, Eq. (13) can be written as

$$\Delta t=\Delta\psi P=\frac{1}{c}\boldsymbol{n}\cdot(\boldsymbol{r}_{t_2}-\boldsymbol{r}_{t_1}). \tag{14}$$

4 Weighted least squares method to determine the initial orbit

4.1 Basic theory of spacecraft orbit determination

In general, the expression of the dynamic system measurement model for nonlinear mechanics is

$$\begin{cases}\dot{\boldsymbol{X}}=F(\boldsymbol{X},t),\ \boldsymbol{X}(t_k)\equiv\boldsymbol{X}_k,\\ \boldsymbol{Y}_i=G(\boldsymbol{X}_i,t_i)+\varepsilon_{\mathrm{i}},\quad i=1,2,\ldots,n,\end{cases} \tag{15}$$

where $\boldsymbol{X}_k$ is the n-dimensional unknown state vector at time t_k, and $\boldsymbol{Y}_i$ is the p-dimensional observation vector to acquire the best estimation of $\boldsymbol{X}_k$, i.e., $\hat{\boldsymbol{X}}_k$.

Spacecraft orbit determination can be regarded as a nonlinear estimation problem. The system function should be linearized before it can be solved by linear estimation theory.

Suppose there is a reasonable reference trajectory $\boldsymbol{X}^*$ and the real orbit $\boldsymbol{X}$. Then the orbit of actual movement can be expanded in a Taylor series about reference orbit in a certain period. If the higher-order terms of Taylor series expansion are ignored, the relationship between the real and reference trajectories can be described by a linear difference equation, which depends only on the time.

Let $\boldsymbol{x}$ be the n-dimensional state difference matrix and $\boldsymbol{y}$ the p-dimensional observation difference matrix. Here, $\boldsymbol{x}$ and $\boldsymbol{y}$ are defined as

$$\begin{cases} \boldsymbol{x}(t)=\boldsymbol{X}(t)-\boldsymbol{X}^*(t), \\ \boldsymbol{y}(t)=\boldsymbol{Y}(t)-\boldsymbol{Y}^*(t), \\ \dot{\boldsymbol{x}}(t)=\dot{\boldsymbol{X}}(t)-\dot{\boldsymbol{X}}^*(t). \end{cases} \tag{16}$$

Expanding Eq. (15) into a Taylor series with respect to the reference point, the following equations are obtained:

$$\begin{aligned} &\dot{\boldsymbol{X}}(t)=F(\boldsymbol{X},t)=F(\boldsymbol{X}^*,t) \\ &+\left[\frac{\partial F(t)}{\partial \boldsymbol{X}(t)}\right]^*\left[\boldsymbol{X}(t)-\boldsymbol{X}^*(t)\right]+O_F\left[\boldsymbol{X}(t)-\boldsymbol{X}^*(t)\right], \\ &\boldsymbol{Y}_i=G(\boldsymbol{X}_i,t_i)+\varepsilon_i=G(\boldsymbol{X}_i^*,t_i) \\ &+\left[\frac{\partial G}{\partial \boldsymbol{X}}\right]_i^*\left[\boldsymbol{X}(t_i)-\boldsymbol{X}^*(t_i)\right]_i+O_G\left[\boldsymbol{X}(t_i)-\boldsymbol{X}^*(t_i)\right]+\varepsilon_i, \end{aligned} \tag{17}$$

where $[\cdot]^*$ indicates the partial derivative of matrix, $\boldsymbol{X}^*(t)$ is the reference solution, which can be obtained by integrating Eq. (15) with the specific initial condition $\boldsymbol{X}^*(t_0)$, and O_F and O_G are the higher-order Taylor series of $\boldsymbol{X}$ and $\boldsymbol{Y}_i$, respectively. Assume that the higher-order terms are far less than the first-order term, and thus they can be neglected.

If the condition meets

$$\begin{cases} \dot{\boldsymbol{X}}^*=F(\boldsymbol{X}^*,t), \\ \boldsymbol{Y}_i^*=G(\boldsymbol{X}_i^*,t_i), \end{cases} \tag{18}$$

Eq. (15) can be rewritten as

$$\begin{cases} \dot{\boldsymbol{x}}(t)=\boldsymbol{A}(t)\boldsymbol{x}(t), \\ \boldsymbol{y}_i=\tilde{\boldsymbol{H}}_i\boldsymbol{x}_i+\varepsilon_i, \quad i=1,2,\ldots,n, \end{cases} \tag{19}$$

where $\boldsymbol{A}(t)=\left[\partial F(t)/\partial \boldsymbol{X}(t)\right]^*$ and $\tilde{\boldsymbol{H}}_i=\left[\partial G/\partial \boldsymbol{X}\right]_i^*$.

Thus, the original nonlinear estimation problem turns into a linear estimation problem described by Eq. (19). The general solution of the first formula in Eq. (19) can be expressed as

$$\boldsymbol{x}(t)=\boldsymbol{\Phi}(t,t_k)\boldsymbol{x}_k, \tag{20}$$

where $\boldsymbol{x}_k$ is the value of $\boldsymbol{x}(t_k)$ and $\boldsymbol{\Phi}(t, t_k)$ is the state transition matrix for the two-body problem. According to the matrix eigenvalue and eigenvector method, $\boldsymbol{\Phi}(t, t_k)$ can be calculated by

$$\boldsymbol{\Phi}(t,t_0)=\boldsymbol{V}\mathrm{e}^{\lambda(t,t_0)}\boldsymbol{V}^{-1}, \tag{21}$$

where

$$\mathrm{e}^{\lambda(t,t_0)}=\begin{bmatrix} \mathrm{e}^{\lambda_1(t-t_0)} & 0 & \cdots & 0 \\ 0 & \mathrm{e}^{\lambda_2(t-t_0)} & \cdots & 0 \\ \vdots & \vdots & & \vdots \\ 0 & 0 & \cdots & \mathrm{e}^{\lambda_n(t-t_0)} \end{bmatrix},$$

$\lambda_1, \lambda_2, \ldots, \lambda_n$ are the eigenvalues of $\boldsymbol{A}$, and $\boldsymbol{V}$ is a set of linearly independent eigenvectors corresponding to $\lambda_1, \lambda_2, \ldots, \lambda_n$.

4.2 Initial orbit determination based on WLS

According to the two-body motion of the spacecraft in the orbital coordinate system, we can construct a model of the two-body motion of the spacecraft. Based on the theoretical knowledge in Section 4.1, if matrices $\boldsymbol{A}$ and $\tilde{\boldsymbol{H}}$ are already known, the initial orbit can be estimated by the WLS method.

It is assumed that the spacecraft is affected only by the center attraction, without regarding the influence of other inertia forces. Thus, the state vector can be represented as

$$\boldsymbol{X}=[x\ \ y\ \ z\ \ u\ \ v\ \ w]^{\mathrm{T}}. \tag{22}$$

Here, (x, y, z) and (u, v, w) are the position and velocity vectors of the spacecraft at any point,

respectively. According to the two-body motion equation, we can obtain

$$\begin{cases}\ddot{x}=-\mu x/r^3,\\ \ddot{y}=-\mu y/r^3,\\ \ddot{z}=-\mu z/r^3,\end{cases} \tag{23}$$

where μ is the gravitational constant and r the distance between the spacecraft and the Earth center. By Eq. (23), the derivative of $\boldsymbol{X}$ is obtained:

$$\begin{aligned}\dot{\boldsymbol{X}}&=[\dot{x}\ \ \dot{y}\ \ \dot{z}\ \ \dot{u}\ \ \dot{v}\ \ \dot{w}]^{\mathrm{T}}\\ &=[F_1\ \ F_2\ \ F_3\ \ F_4\ \ F_5\ \ F_6]^{\mathrm{T}}\\ &=[u\ \ v\ \ w\ \ -\mu x/r^3\ \ -\mu y/r^3\ \ -\mu z/r^3]^{\mathrm{T}}.\end{aligned} \tag{24}$$

According to Eq. (19),

$$\boldsymbol{A}(t)=\frac{\partial F(\boldsymbol{X},t)}{\partial \boldsymbol{X}}$$

$$=\begin{bmatrix}0 & 0 & 0 & 1 & 0 & 0\\ 0 & 0 & 0 & 0 & 1 & 0\\ 0 & 0 & 0 & 0 & 0 & 1\\ -\frac{\mu}{r^3}+\frac{3\mu x^2}{r^5} & \frac{3\mu xy}{r^5} & \frac{3\mu xz}{r^5} & 0 & 0 & 0\\ \frac{3\mu xy}{r^5} & -\frac{\mu}{r^3}+\frac{3\mu y^2}{r^5} & \frac{3\mu yz}{r^5} & 0 & 0 & 0\\ \frac{3\mu zx}{r^5} & \frac{3\mu yz}{r^5} & -\frac{\mu}{r^3}+\frac{3\mu z^2}{r^5} & 0 & 0 & 0\end{bmatrix}. \tag{25}$$

According to Eq. (21), $\boldsymbol{\Phi}(t_j, t_k)$ can be obtained as

$$\boldsymbol{\Phi}(t_j,t_k)=\begin{bmatrix}0 & 0 & 0 & 1 & 0 & 0\\ 0 & 0 & 0 & 0 & 1 & 0\\ 0 & 0 & 0 & 0 & 0 & 1\\ -\frac{\mu}{r^3}+\frac{3\mu x^2}{r^5} & \frac{3\mu xy}{r^5} & \frac{3\mu xz}{r^5} & 0 & 0 & 0\\ \frac{3\mu xy}{r^5} & -\frac{\mu}{r^3}+\frac{3\mu y^2}{r^5} & \frac{3\mu yz}{r^5} & 0 & 0 & 0\\ \frac{3\mu zx}{r^5} & \frac{3\mu yz}{r^5} & -\frac{\mu}{r^3}+\frac{3\mu z^2}{r^5} & 0 & 0 & 0\end{bmatrix}\cdot T_{jk}, \tag{26}$$

where $T_{jk}=t_j-t_k$. According to Eq. (11), the observation is denoted by

$$Z_i=t_i=P_i\psi=\hat{\boldsymbol{n}}_i\cdot\boldsymbol{x}_i/c. \tag{27}$$

In this study, the newly introduced observation is the time increment, defined as $\hat{T}_{kj}=\hat{\boldsymbol{n}}_i\cdot(\boldsymbol{x}_k-\boldsymbol{x}_j)/c$, and the observation function can be redefined by

$$\boldsymbol{Z}=[Z_1\ Z_2\ \hat{T}_{21}\ Z_3\ Z_4\ \hat{T}_{43}\ \cdots], \tag{28}$$

which can also be expressed as

$$\begin{cases}y_1=Z_1=\dot{\boldsymbol{H}}_1\boldsymbol{\Phi}(t_1,t_k)\boldsymbol{x}_k+\varepsilon_1,\\ y_2=Z_2=\dot{\boldsymbol{H}}_2\boldsymbol{\Phi}(t_2,t_k)\boldsymbol{x}_k+\varepsilon_2,\\ y_3=\hat{T}_{21}=\dot{\boldsymbol{H}}_2(\boldsymbol{\Phi}(t_2,t_k)-\boldsymbol{\Phi}(t_1,t_k))\boldsymbol{x}_k+\varepsilon_3,\\ \quad\vdots\\ y_i=Z_j=\dot{\boldsymbol{H}}_j\boldsymbol{\Phi}(t_j,t_k)\boldsymbol{x}_k+\varepsilon_i.\end{cases} \tag{29}$$

We can denote the elements in Eq. (29) as

$$\boldsymbol{y}\equiv\begin{bmatrix}y_1\\ y_2\\ \vdots\\ y_l\end{bmatrix},\ \boldsymbol{H}\equiv\begin{bmatrix}\dot{\boldsymbol{H}}_1\boldsymbol{\Phi}(t_1,t_k)\\ \dot{\boldsymbol{H}}_2\boldsymbol{\Phi}(t_1,t_k)\\ \vdots\\ \dot{\boldsymbol{H}}_i\boldsymbol{\Phi}(t_1,t_k)\end{bmatrix},\ \hat{\boldsymbol{I}}\equiv\begin{bmatrix}\varepsilon_1\\ \varepsilon_2\\ \vdots\\ \varepsilon_i\end{bmatrix}, \tag{30}$$

where ε_1, ε_2, …, ε_i are the differences between the theoretical and observed values of the measurement error, which are generally considered to be of the white noise distribution and not related to each other.

If the characteristic value and eigenvector of matrix $\boldsymbol{A}$ are known, $\boldsymbol{\Phi}(t, t_0)$ can be calculated. Then we can estimate the state vectors of the spacecraft by WLS, and the best estimation of state vector is

$$\hat{\boldsymbol{x}}=(\boldsymbol{H}^{\mathrm{T}}\boldsymbol{w}\boldsymbol{H})^{-1}\boldsymbol{H}^{\mathrm{T}}\boldsymbol{w}\boldsymbol{y}, \tag{31}$$

where $\boldsymbol{w}=\mathrm{diag}(\varepsilon_1^{-2},\varepsilon_2^{-2},\ldots,\varepsilon_i^{-2})$.

5 Simulation

In the simulation, three different orbits are adopted to verify the method proposed in this study.

The parameters of the orbits are shown in Table 1. The detector observes three pulsars in turn to determine the initial orbit of the satellite. These pulsars are B0531+21, B1937+21, and B0329+54 (Sheikh, 2005). Considering that different initial position errors and speed errors have different influence on the initial orbit determination precision, a detailed simulation with initial position errors changing from 0.1 to 10 km and speed errors with different values of 0.5, 2.0, and 5.0 m/s is carried out. After 100 Monte Carlo simulations, the mean error and mean square error of the initial orbit are obtained to evaluate the performance of the proposed method.

Two kinds of methods are applied to determine the spacecraft's initial orbit. The first one observes three X-ray pulsars in turn to obtain three TDOAs of the pulsars, and the second one adds a phase increment observation to the TDOAs.

First, the GPS BIIA-10 orbit is selected for the simulation. The estimation results of the height and velocity for the initial orbit determination are obtained. From Fig. 3, it can be seen that when the initial velocity error δv is 0.5, 2.0, and 5.0 m/s, respectively, and the initial position error is arbitrarily set between 0.1 and 10 km, the new method combining the phase increment has a better performance than the method without phase increment. A more detailed simulation of data, shown in Table 2, indicates that the position precision obtained by the new method with phase increment has been improved by nearly 40% and the velocity precision by more than 50%.

For the second situation, the TestSatOrbit is selected. From Fig. 4 and Table 3, it can be seen that when the satellite is moving along the middle height orbit (TestSatOrbit), the new method with phase increment has a better performance than that without phase increment. Table 3 also shows an improvement on the precisions of position and velocity of 30% and 20%, respectively.

Third, the MEGSAT-1 orbit is selected in the simulation. Fig. 5 indicates that the new method with phase increment observation has a better accuracy

Table 1 Orbit parameters setting during the simulation

Orbit name	Semimajor axis (km)	Right ascension of ascending node (°)	Orbit eccentricity	Argument of perigee (°)	Orbital inclination (°)
GPS BIIA-10	26 560.5	224.67	0.0116	338.24	54.39
TestSatOrbit	15 000.0	150.00	0.0050	45.00	22.00
MEGSAT-1	6994.3	341.25	0.0049	281.70	64.56

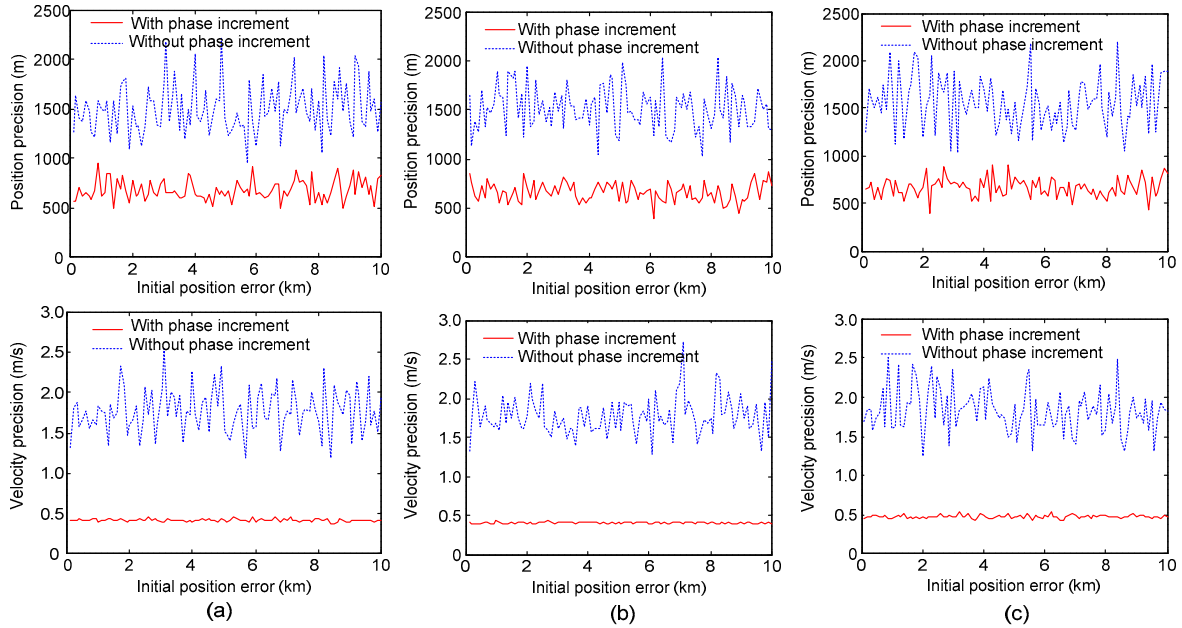

Fig. 3 Position and velocity precision in the simulation of GPS BIIA-10 initial orbit determination: (a) δv=0.5 m/s; (b) δv=2.0 m/s; (c) δv=5.0 m/s

Table 2 Estimation results of the height and speed error for GPS BIIA-10 orbit

Initial speed error (m/s)	Mean error of position (km)		RMSE of position (km)		Mean error of velocity (m/s)		RMSE of velocity (m/s)	
	WOPI	WPI	WOPI	WPI	WOPI	WPI	WOPI	WPI
0.5	1.4868	0.6435	0.2237	0.0922	1.7824	0.4021	0.2179	0.0216
2.0	1.5168	0.6580	0.2243	0.0950	1.7511	0.4268	0.2600	0.0220
5.0	1.5654	0.6691	0.2676	0.1003	1.8297	0.4762	0.2748	0.0211

RMSE: root mean square error, WOPI: new method without phase increment, WPI: new method with phase increment

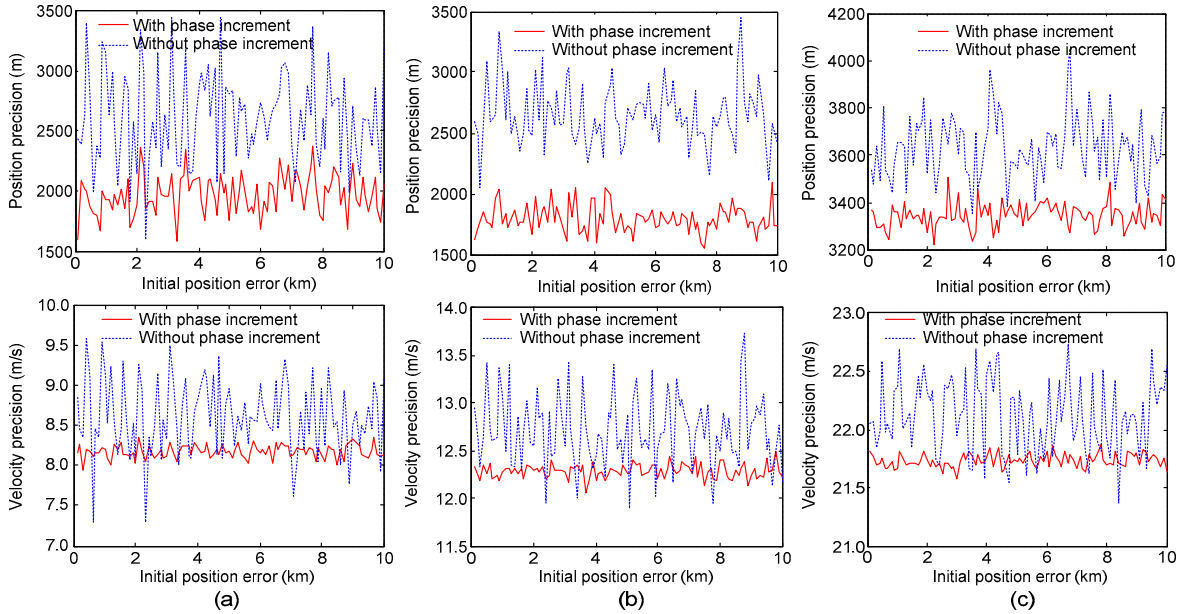

Fig. 4 Position and velocity precision in the simulation of TestSatOrbit initial orbit determination: (a) δ*v*=0.5 m/s; (b) δ*v*=2.0 m/s; (c) δ*v*=5.0 m/s

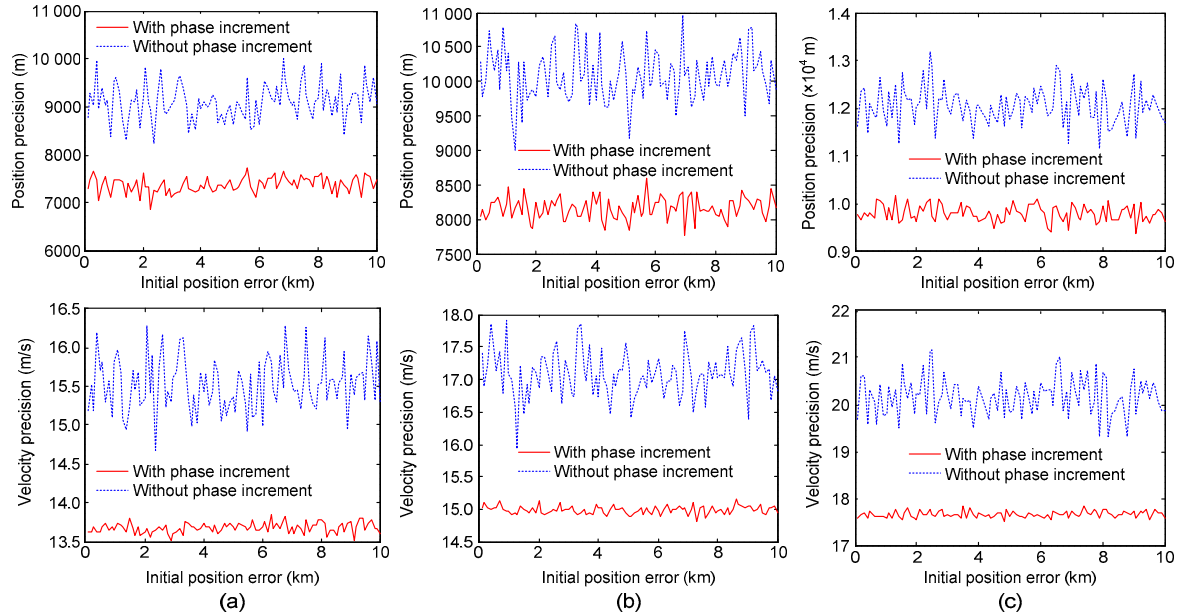

Fig. 5 Position and velocity precision in the simulation of MEGSAT-1 initial orbit determination: (a) δ*v*=0.5 m/s; (b) δ*v*=2.0 m/s; (c) δ*v*=5.0 m/s

Table 3 Estimation results of the height and speed error for TestSatOrbit

Initial speed error (m/s)	Mean value of position (km)		RMSE of position (km)		Mean value of velocity (m/s)		RMSE of velocity (m/s)	
	WOPI	WPI	WOPI	WPI	WOPI	WPI	WOPI	WPI
0.5	1.6677	1.0201	0.1587	0.0904	2.8296	2.5583	0.2296	0.0115
2.0	1.6807	1.1199	0.2389	0.1308	2.8973	2.7464	0.3340	0.0174
5.0	1.7853	1.2550	0.2777	0.1369	3.2113	3.1189	0.4166	0.0184

RMSE: root mean square error, WOPI: new method without phase increment, WPI: new method with phase increment

Table 4 Estimation results of the height and speed error for MEGSAT-1 orbit

Initial speed error (m/s)	Mean value of position (km)		RMSE of position (km)		Mean value of velocity (m/s)		RMSE of velocity (m/s)	
	WOPI	WPI	WOPI	WPI	WOPI	WPI	WOPI	WPI
0.5	9.1279	7.3427	0.2497	0.0997	15.5233	13.6060	0.2194	0.0088
2.0	10.1043	8.0917	0.3793	0.1555	17.0824	14.8990	0.3420	0.0136
5.0	12.0779	9.7202	0.4058	0.1698	20.1775	17.5714	0.3861	0.0145

RMSE: root mean square error, WOPI: new method without phase increment, WPI: new method with phase increment

than the method without phase increment. The position precision is improved by 20% and velocity by 15% (Table 4). From Tables 2–4, we can find that the precisions of position and velocity decrease with increase in the initial velocity error. Another conclusion is that, for the low satellite orbit (e.g., MEGSAT-1 orbit), the position and speed precisions of both methods decrease. It is because the error of the state propagation function increases in a low Earth orbit due to the high speed of the satellite, and the observation time of TOA should always be no less than 500 s to obtain a sufficiently large signal-to-noise ratio (SNR). If only one detector is installed on the satellite, three pulsars will be observed in turn, and therefore the observation time will be longer. During a longer observation time, a small initial speed error of the satellite moving at a high speed will result in a large position error.

6 Conclusions

In this paper, we showed that only one detector is needed to observe different pulsars in turn for the navigation of a satellite. The phase increments of the satellite at different adjoining instants were used to improve the navigation. The simulation results indicated that the method combined with phase increment observation gives better performance than that without phase increment. The precision of position is improved by more than 30% and the velocity by more than 20% with the new method. This initial orbit determination precision of this new method meets the rough initial determination requirement and provides a potential strategy for the following higher precision orbit determination.

References

Backer, D.C., Hellings, R.W., 1986. Pulsar timing and general relativity. *Ann. Rev. Astron. Astrophys.*, **24**:537-575. http://dx.doi.org/10.1146/annurev.aa.24.090186.002541

Chester, T.J., Butman, S.A., 1981. Navigation Using X-ray Pulsars. The Telecommunications and Data Acquisition Progress Report No. TDA PR 42-63, NASA, p.22-25.

Deutschmann, J.K., Bar-Itzhack, I.Y., 2001. Evaluation of attitude and orbit estimation using actual earth magnetic field data. *J. Guid. Contr. Dyn.*, **24**(3):616-623. http://dx.doi.org/10.2514/2.4753

Emadzadeh, A.A., Speyer, J.L., 2011. Relative navigation between two spacecraft using X-ray pulsars. *IEEE Trans. Contr. Syst. Technol.*, **19**(5):1021-1035. http://dx.doi.org/10.1109/TCST.2010.2068049

Farahanifar, M., Assadian, N., 2015. Integrated magnetometer—horizon sensor low-Earth orbit determination using UKF. *Acta Astronaut.*, **106**:13-23. http://dx.doi.org/10.1016/j.actaastro.2014.10.007

Hinedi, S., 1993. NASA's next generation all-digital deep space network breadboard receiver. *IEEE Trans. Commun.*, **41**(1):246-257. http://dx.doi.org/10.1109/26.212383

Huang, L.W., Liang, B., 2010. Autonomous initial orbit determination of high-Earth-orbit satellites using X-ray pulsars. *J. Syst. Simul.*, **22**(S1):258-261 (in Chinese) .

Liu, J., Fang, J.C., Yang, Z.H., *et al.*, 2015. X-ray pulsar/Doppler difference integrated navigation for deep space exploration with unstable solar spectrum. *Aerosp.*

Sci. Technol., **41**:144-150. http://dx.doi.org/10.1016/j.ast.2014.11.019

Ma, J., Xu, J., Cao, Z.B., 2005. A method of autonomous orbit determination for satellite using star sensor. *Sci. China Ser. G*, **48**(3):268-281. http://dx.doi.org/10.1360/142004-23

Mao, Y., Chen, J.P., Song, X.Y., 2010. Single X-ray pulsar dynamic orbit determination. *J. Geomat. Sci. Technol.*, **27**(4):251-254 (in Chinese).

Psiaki, M.L., 1995. Autonomous orbit and magnetic field determination using magnetometer and star sensor data. *J. Guid. Contr. Dyn.*, **18**(3):584-592. http://dx.doi.org/10.2514/3.21427

Qian, Y., Li, C., Jing, W., *et al.*, 2013. Sun-Earth-Moon autonomous orbit determination for quasi-periodic orbit about the translunar libration point and its observability analysis. *Aerosp. Sci. Technol.*, **28**(1):289-296. http://dx.doi.org/10.1016/j.ast.2012.11.009

Ray, P.S., Wood, K.S., Wolff, M.T., *et al.*, 2002. Absolute timing of the crab pulsar: X-ray, radio, and optical observations. *Bull. Am. Astron. Soc.*, **34**:1298.

Shang, L., Liu, G., Zhang, R., *et al.*, 2013. An information fusion algorithm for integrated autonomous orbit determination of navigation satellites. *Acta Astronaut.*, **85**: 33-40. http://dx.doi.org/10.1016/j.actaastro.2012.12.007

Sheikh, S.I., 2005. The Use of Variable Celestial X-ray Sources for Spacecraft Navigation. PhD Thesis, University of Maryland, College Park, USA.

Sheikh, S.I., Hellings, R.W., Matzner, R.A., 2007. High-order pulsar timing for navigation. 63rd Annual Meeting of the Institute of Navigation, p.432-443.

Sheikh, S.I., Hanson, J.E., Graven, P.H., *et al.*, 2011. Spacecraft navigation and timing using X-ray pulsars. *Navigation*, **58**(2):165-186. http://dx.doi.org/10.1002/j.2161-4296.2011.tb01799.x

Taylor, J.H., 1992. Pulsar timing and relativistic gravity. *Phil. Trans. Phys. Sci. Eng.*, **341**(1660):117-134.

Visser, P.N.A.M., van den Ijssel, J., 2000. GPS-based precise orbit determination of the very low Earth-orbiting gravity mission GOCE. *J. Geod.*, **74**(7):590-602. http://dx.doi.org/10.1007/s001900000119

Wang, Y., Zheng, W., Sun, S., *et al.*, 2013. X-ray pulsar-based navigation system with the errors in the planetary ephemerides for Earth-orbiting satellite. *Adv. Space Res.*, **51**(12):2394-2404. http://dx.doi.org/10.1016/j.asr.2013.02.007

Woodfork, D.W., 2005. The Use of X-ray Pulsars for Aiding GPS Satellite Orbit Determination. MS Thesis, Air University, Maxwell Air Force Base, USA.

Xiong, K., Wei, C., Liu, L., 2013. Autonomous navigation for a group of satellites with star sensors and inter-satellite links. *Acta Astronaut.*, **86**:10-23. http://dx.doi.org/10.1016/j.actaastro.2012.12.001

Zhang, H., Xu, L., 2011. An improved phase measurement method of integrated pulse profile for pulsar. *Sci. China Technol. Sci.*, **54**(9):2263-2270. http://dx.doi.org/10.1007/s11431-011-4524-8

Zhang, H., Xu, L., Shen, Y., *et al.*, 2014. A new maximum-likelihood phase estimation method for X-ray pulsar signals. *J. Zhejiang Univ.-Sci. C (Comput. & Electron.)*, **15**(6):458-469. http://dx.doi.org/10.1631/jzus.C1300347